J. Fluid Mech. (2014), *vol.* 749, *pp.* 167–183.
doi:10.1017/jfm.2014.214

Electro-osmotic flow through a nanopore

M. Mao[1], J. D. Sherwood[3] and S. Ghosal[1,2,†]

[1]Department of Mechanical Engineering, Northwestern University, 2145 Sheridan Rd, Evanston, IL 60208, USA

[2]Department of Engineering Sciences and Applied Mathematics, Northwestern University, 2145 Sheridan Rd, Evanston, IL 60208, USA

[3]Department of Applied Mathematics and Theoretical Physics, University of Cambridge, Wilberforce Road, Cambridge CB3 0WA, UK

(Received 13 December 2013; revised 2 April 2014; accepted 12 April 2014; first published online 14 May 2014)

Electro-osmotic pumping of fluid through a nanopore that traverses an insulating membrane is considered. The density of surface charge on the membrane is assumed to be uniform and sufficiently low for the Poisson–Boltzmann equation to be linearized. The reciprocal theorem gives the flow rate generated by an applied weak electric field, expressed as an integral over the fluid volume. For a circular hole in a membrane of zero thickness, an analytical result is possible up to quadrature. For a membrane of arbitrary thickness, the full Poisson–Nernst–Planck–Stokes system of equations is solved numerically using a finite volume method. The numerical solution agrees with the standard analytical result for electro-osmotic flux through a long cylindrical pore when the membrane thickness is large compared to the hole diameter. When the membrane thickness is small, the flow rate agrees with that calculated using the reciprocal theorem.

Key words: electrohydrodynamic effects, microfluidics, MEMS/NEMS

1. Introduction

A nanopore is simply a hole of small size in an impermeable membrane that separates two regions containing an electrolytic buffer. A size range of 1–100 nm is fairly typical. Living cells and intracellular organelles are usually bounded by lipid membranes containing nanopores constructed of membrane-bound proteins. The transport of small molecules and polymers across such nanopores is a very common feature of living cells and is essential to their normal function (Pfanner & Neupert 1990; Martin, Mahlke & Pfanner 1991; Alberts *et al.* 1994; Künkele, Heins & Dembowski 1998; Matouschek, Pfanner & Voos 2000). Synthetic nanopores (Li *et al.* 2003; Storm *et al.* 2005*a*,*b*; Smeets *et al.* 2006; Garaj *et al.* 2010; Hall *et al.* 2010; Schneider *et al.* 2010) have been the focus of much interest in recent years, following the demonstration of their use as effective single-molecule sensors (Kasianowicz *et al.* 1996).

The main distinguishing feature of nanopore systems responsible for many of the novel effects is that their geometric dimensions are small enough that electrokinetic

† Email address for correspondence: s-ghosal@u.northwestern.edu

effects are important. Such effects have been invoked to explain a range of observations relating to experiments involving free as well as hindered translocation of DNA across synthetic nanopores (Ghosal 2006; Keyser *et al.* 2006; Ghosal 2007*a*,*b*; van Dorp *et al.* 2009; Laohakunakorn *et al.* 2013*b*). Nanopores also exhibit other unusual properties, some of which could potentially be exploited to build novel microfluidic devices. For example, conical nanopores fabricated on plastic films using the ion track-etching technique (Siwy 2006) have been shown to exhibit ion current rectification similar to that of semiconductor diodes (Siwy & Fulinsski 2004; Vlassiouk & Siwy 2007; Vlassiouk, Smirnov & Siwy 2008*a*,*b*). A similar effect has been reported recently for electro-osmotic flow out of nanocapillaries (Laohakunakorn *et al.* 2013*b*). A nonlinear electrokinetic effect known as induced charge electro-osmosis (ICEO) (Murtsovkin 1996; Squires & Bazant 2004) produces vortices at the edges of nanopores which resemble recirculation vortices in separated flows, even though the Reynolds number in such applications is essentially zero. Mixing due to these flow structures (Yossifon & Chang 2008; Chang & Yossifon 2009; Chang, Yossifon & Demekhin 2012) and electroconvective instabilities (Zaltzman & Rubinstein 2007) are thought to be responsible for the 'overlimiting' behaviour of the current–voltage characteristics of perm-selective pores and membranes described by Rubinstein & Shtilman (1979). Similar vortical structures may be generated in cylindrical channels that undergo a sudden constriction when the relevant length scales are of the order of the Debye length (Park *et al.* 2006).

If an electric field E is applied across an uncharged membrane, ICEO leads to velocities of $O(E^2)$ with no net flow through the membrane unless symmetry is somehow broken. Molecular dynamics simulations of flow through nanopores in uncharged membranes, such as graphene sheets (Hu, Mao & Ghosal 2012), show that differences in mobility between cations and anions can result in asymmetric Debye layers and consequent net flow through the membrane. Symmetry is also broken if the membrane is charged, so that the intrinsic field due to the membrane competes with the externally applied field in determining the distribution of ions in the Debye layer (Mao, Ghosal & Hu 2013).

If a voltage is applied across a charged membrane containing a long narrow pore, an electro-osmotic flow is generated by the electric field acting on the charge cloud of counter-ions in the fluid adjacent to the fixed charges at the solid–fluid interface. The strength of this flow is proportional to the applied electric field and, thus, inversely proportional to the membrane thickness if the membrane is sufficiently thick. However, the flow does not increase indefinitely as the membrane is progressively thinned. If the membrane is much thinner than the diameter of the hole, the flow is driven mainly by electro-osmosis at the membrane surface exterior to the pore, rather than by electric forces within the pore itself.

Here we present results for the flow rate through a pore in a charged membrane in the limit of a weak applied field. In § 2 we use the reciprocal theorem to calculate the flow rate through a circular hole in a charged membrane of zero thickness. The result is obtained in terms of an integral which in general has to be evaluated numerically but can be calculated analytically when the pore size is much smaller than the Debye length. In § 3 we present computer simulations of the full problem based on numerical solutions of the Poisson–Nernst–Planck–Stokes (PNP–Stokes) system of equations using a finite volume method. Both thick and thin membranes are considered, and the results are compared with analytical results for membranes of zero thickness and of large thickness relative to the pore radius. Conclusions are provided in § 4.

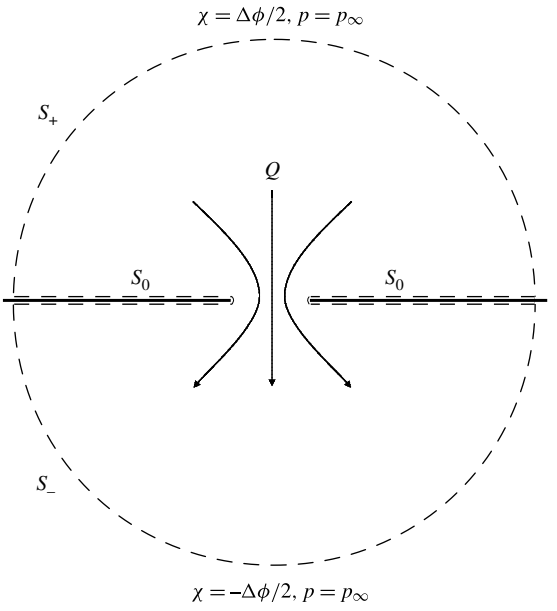

FIGURE 1. Flow through a charged membrane under an applied potential difference $\Delta\phi$.

2. Flow through a hole in a membrane of zero thickness

We consider a hole (of arbitrary shape) in an infinite plane membrane immersed in an incompressible homogeneous electrolyte containing N ionic species (figure 1). The number density of the ith ionic species is n^i, with $n^i = n^i_\infty$ in the bulk electrolyte far from any charged surfaces. The electrolyte has viscosity μ and electrical permittivity ϵ. A surface charge of fixed density σ exists at the membrane–electrolyte interface, and in the electrolyte adjacent to the membrane there is charge cloud of counter-ions, with thickness characterized by the Debye length

$$\kappa^{-1} = \left(\frac{\epsilon kT}{\sum_{i=1}^{N} e^2 z_i^2 n^i_\infty} \right)^{1/2}, \tag{2.1}$$

where k is the Boltzmann constant, T the absolute temperature, e the proton charge and z_i the valence of the ith species of ion. We assume that the surface charge density σ is sufficiently small so that the Poisson–Boltzmann equation describing the potential ϕ_0 in the equilibrium charge cloud may be linearized. Far from any hole in the membrane, the zeta potential at the surface of the membrane is $\zeta = \sigma/(\epsilon\kappa)$, with $\zeta \ll kT/e$. An electric potential difference $\Delta\phi$ is applied across the membrane with a resulting current I. The hole within the membrane has characteristic size a, and we make no assumption concerning $a\kappa$, the ratio of the hole size to the Debye length κ^{-1}. When $a\kappa \ll 1$, the charge clouds from opposite sides of the perimeter of the hole overlap, but this has little effect on the electrical conductivity of the hole when (as here) the surface charge density σ and the resulting perturbations to the ionic number densities $n^i = n^i_\infty \exp(-ez_i\phi/kT)$ are small. Similarly, any ion exclusion effects of

the overlapping charge cloud are negligible. We also note that the ion exclusion properties of a thin membrane are in general smaller than those of a long cylindrical pore. When $a\kappa \ll 1$, the potential in the unperturbed electrical double layer within the pore, on the plane of the membrane, is $\zeta \approx \sigma/(\epsilon\kappa)$. Inside a uniform cylindrical pore with surface charge density σ, the potential when $a\kappa \ll 1$ is $\zeta \approx 2\sigma/(\epsilon a\kappa^2)$, and the condition $e\zeta/kT \ll 1$ required for the perturbation of the ionic number densities to be small within the pore implies a smaller charge density σ for the pore than for the membrane. Only when $a\kappa = O(1)$ will the long cylindrical pore and the hole in a membrane exhibit similar ion exclusion properties.

When $a\kappa \gg 1$, the charge cloud is thin compared to the lateral dimension of the hole, but it remains thick compared to the membrane of zero thickness, $h = 0$, considered in § 2.3. Thus, we are unable to appeal to Smoluchowski's analysis for thin charge clouds in § 2.3. Ion exclusion effects are negligible in this limit.

In § 2.1 we discuss how the charge cloud is deformed by the applied electric field and by fluid motion. We then (in § 2.2) describe a theoretical framework for calculating the flow rate Q through the hole, exploiting the reciprocal theorem; the analysis is similar to that of Sherwood & Stone (1995). In § 2.3 we consider the special case of a circular hole in a thin membrane, for which the integral for the flow rate Q can be computed numerically.

2.1. *The perturbed charge cloud*

When the electrical potential difference $\Delta\phi$ is applied across the membrane, the charge cloud adjacent to the surface of the membrane is perturbed, both by the direct electrical field $\nabla\phi$ acting on the ions and by motion of the fluid. Ions are convected with the fluid velocity $\boldsymbol{u}$, and move relative to the fluid under the influence of electric fields and thermal diffusion. The conservation equation for the number density n^i of the ith ionic species, in steady state, is therefore

$$\nabla \cdot \left[n^i \boldsymbol{u} - \omega^i (kT\nabla n^i + e z_i n^i \nabla\phi)\right] = 0, \tag{2.2}$$

where ω^i is the mobility of the ith species of ion.

We follow Saville (1977) and non-dimensionalize potentials by kT/e, lengths by the typical hole dimension a, velocities by $\epsilon(kT/e)^2/\mu a$ and mobilities by a characteristic mobility value ω^0. We assume that the potential $\Delta\phi$ which characterizes the applied field is small compared to the equilibrium zeta potential ζ, so that $\beta = e\Delta\phi/kT \ll e\zeta/kT$, where $e\zeta/kT$ has already been assumed small in order that we may describe the charge cloud by means of the linearized Poisson–Boltzmann equation. We use the dimensionless field strength β as the basis for a perturbation expansion

$$\hat{\boldsymbol{u}} = \beta\hat{\boldsymbol{u}}_1 + \cdots, \tag{2.3a}$$

$$\hat{\phi} = \hat{\phi}_0 + \beta\hat{\phi}_1 + \cdots, \tag{2.3b}$$

$$n^i = n^i_0 + \beta n^i_1 + \cdots, \tag{2.3c}$$

where the subscript 0 refers to the equilibrium cloud and the caret $\hat{}$ denotes a non-dimensional quantity. The steady-state ion conservation equation, correct to $O(\beta)$, becomes

$$Pe\,\hat{\boldsymbol{u}}_1 \cdot \nabla n^i_0 = \hat{\omega}^i \nabla \cdot \left[z_i n^i_0 \nabla\hat{\phi}_1 + z_i n^i_1 \nabla\hat{\phi}_0 + \nabla n^i_1\right], \tag{2.4}$$

where the Péclet number $Pe = \epsilon kT/e^2\mu\omega^0$ characterizes the ratio of ionic convection to diffusion. Since the non-dimensional equilibrium potential $\hat{\phi}_0$ has been assumed to be small, (2.4) reduces to

$$0 = z_i n^i_\infty \nabla^2 \hat{\phi}_1 + \nabla^2 n^i_1. \tag{2.5}$$

The boundary conditions at infinity are

$$n^i_1 \to 0, \tag{2.6a}$$

$$\beta\phi_1 \sim \pm\Delta\phi/2 \quad \text{in } z \gtrless 0. \tag{2.6b}$$

We assume that no ions enter or leave the surface of the membrane. Hence

$$\boldsymbol{n} \cdot (kT\nabla n^i + ez_i n^i \nabla\phi) = 0, \tag{2.7}$$

where $\boldsymbol{n}$ is the normal to the membrane. At $O(\beta)$, and assuming $\hat{\phi}_0 \ll 1$, this zero-flux boundary condition becomes

$$\boldsymbol{n} \cdot \nabla \left(n^i_1 + z_i n^i_\infty \hat{\phi}_1 \right) = 0. \tag{2.8}$$

Multiplying (2.5) by $e^2 z_i$ and summing over i, we obtain, at $O(\beta)$,

$$\nabla^2 \hat{\chi}_1 = 0, \tag{2.9}$$

where

$$\hat{\chi}_1 = \hat{\phi}_1 + \hat{\rho}_1 (a\kappa)^{-2} \tag{2.10}$$

and

$$\hat{\rho}_1 = \frac{ea^2\rho_1}{\epsilon kT} = \frac{ea^2}{\epsilon kT} \sum_{i=1}^{N} ez_i n^i_1 \tag{2.11}$$

is the (non-dimensional) perturbation to the charge density $\rho = \sum_i ez_i n^i$.

The boundary conditions for (2.9) are similarly obtained from (2.6) and (2.8):

$$\hat{\chi}_1 \sim \pm 1/2 \quad \text{as } \boldsymbol{r} \to \infty \text{ in } z \gtrless 0, \tag{2.12a}$$

$$\boldsymbol{n} \cdot \nabla \hat{\chi}_1 = 0 \quad \text{on the membrane}, \tag{2.12b}$$

and we note that the boundary condition (2.12*b*) represents zero flux of ions into the membrane, rather than a zero normal electric field. The potential

$$\chi = \phi_1 + \rho_1/\epsilon\kappa^2 \tag{2.13}$$

is thus obtained by solving the Laplace equation for the potential created by applying the potential difference $\Delta\phi$ across the insulating membrane containing the pore. The potential χ is related to the linearized change $\mu^i_1 = ez_i\phi_1 + kTn^i_1/n^i_\infty$ in the electrochemical potential of the ith species of ion, with $\chi = \sum_i ez_i n^i_\infty \mu^i_1/(\epsilon kT\kappa^2)$. As discussed by Saville (1977), when $\hat{\phi}_0 \ll 1$ the perturbation ρ_1 to the charge density is negligibly small, so that $\phi_1 = \chi$, and our analysis is equivalent to that of Henry (1931).

2.2. *A formalism for calculating the flow rate using the reciprocal theorem*

The Stokes equations governing fluid motion are modified by the presence of an electric force $-\rho\nabla\phi$ acting on the fluid. Expanding in powers of β, we find that

$$\begin{aligned}\rho\nabla\phi &= (\rho_0+\beta\rho_1)\nabla(\phi_0+\beta\phi_1)+O(\beta^2)\\ &= -\nabla\left(\tfrac{1}{2}\epsilon\kappa^2\phi_0^2-\beta\rho_1\phi_0\right)+\beta\rho_0\nabla(\phi_1+\rho_1/\epsilon\kappa^2)+O(\beta^2),\end{aligned}\tag{2.14}$$

where we have used the relation $\rho_0=-\epsilon\kappa^2\phi_0$ between the equilibrium charge density ρ_0 and the equilibrium potential ϕ_0 given by the linearized Poisson–Boltzmann equation. Hence the Stokes equations become

$$\mu\nabla^2\boldsymbol{u}-\nabla p-\rho_0\nabla\chi=\boldsymbol{0},\tag{2.15}$$

where the term $\nabla(\epsilon\kappa^2\phi_0^2/2-\beta\rho_1\phi_0)$ in (2.14) has been incorporated into the pressure p.

Note that the fluid motion caused by direct electrical forces acting on the fluid creates additional deformation of the charge cloud, but, as seen from (2.4), this deformation is $O(\hat{u}_1 Pe\,\hat{\phi}_0)$ and may be neglected when $\hat{\phi}_0$ is small.

We now determine the $O(\beta)$ total volumetric flow rate Q through the pore, created by the electrical force acting on the charge cloud within the fluid. Consider two Stokes flows $\boldsymbol{u}$ and $\bar{\boldsymbol{u}}$ in a volume V with boundary conditions given on the bounding surface S with outward normal $\boldsymbol{n}$. A body force $\boldsymbol{F}$ acts on the fluid, in which the pressure is p, the viscosity is μ, the strain rate tensor is $e_{ij}=(\partial_i u_j+\partial_j u_i)/2$ and the stress tensor is $\tau_{ij}=-p\delta_{ij}+2\mu e_{ij}$. Barred variables represent the corresponding quantities for the second flow $\bar{\boldsymbol{u}}$. The reciprocal theorem (Happel & Brenner 1983) gives the identity

$$\int_V u_i\bar{F}_i\,\mathrm{d}V+\int_S u_i\bar{\tau}_{ij}n_j\,\mathrm{d}S=\int_V\bar{u}_iF_i\,\mathrm{d}V+\int_S\bar{u}_i\tau_{ij}n_j\,\mathrm{d}S.\tag{2.16}$$

We suppose that flow 1 (i.e. $\boldsymbol{u}$) is the flow of interest, namely the electrokinetic flow through a hole in a charged membrane. The body force $\boldsymbol{F}$, by (2.15), is

$$\boldsymbol{F}=-\rho_0\nabla\chi,\tag{2.17}$$

where, by (2.9), $\nabla^2\chi=0$ with boundary conditions (2.12): $\hat{\boldsymbol{n}}\cdot\nabla\chi=0$ on the membrane surface S_0, and $\chi\sim\pm\Delta\phi/2$ on surfaces $S_\pm$ far from the pore (figure 1).

We take flow 2 (i.e. $\bar{\boldsymbol{u}}$) to be that due to a pressure difference Δp imposed across a pore in an uncharged membrane; thus, the body force $\bar{\boldsymbol{F}}$ is zero. Since the Stokes flow equations are linear, we may write

$$\bar{\boldsymbol{u}}=\Delta p\,\boldsymbol{G},\tag{2.18}$$

where $\boldsymbol{G}$ is a function that depends solely on the pore geometry.

We now substitute the two flows into the reciprocal relation (2.16). The bounding surface S is as shown in figure 1; it consists of two hemispheres S_+ and S_- of very large radius R, together with the membrane surface S_0. On S_0 the velocities u_i and $\bar{u}_i$ equal zero, whereas on $S_\pm$ we have $\tau_{ij}\sim-p_\pm\delta_{ij}+O(R^{-3})$ and $\bar{\tau}_{ij}\sim-\bar{p}_\pm\delta_{ij}+O(R^{-3})$, where $p_\pm$ are the pressures at a great distance R from the pore on either side of the membrane. For flow 1, $p_+=p_-=p_\infty$, and for flow 2, $\bar{p}_+-\bar{p}_-=\Delta p$. Substituting (2.17) and (2.18) into (2.16) and cancelling the pressure difference Δp from both sides of the equation, we obtain

$$Q=\int_{S_-}\boldsymbol{u}\cdot\boldsymbol{n}\,\mathrm{d}S=-\int_{S_+}\boldsymbol{u}\cdot\boldsymbol{n}\,\mathrm{d}S=-\int_V\rho_0\boldsymbol{G}\cdot\nabla\chi\,\mathrm{d}V,\tag{2.19}$$

where Q is the volumetric flux of flow 1 from the side S_+ to the side S_- of the membrane.

2.3. *Flow rate from a round hole in elliptic cylindrical coordinates*

We now consider a circular pore of radius a. We adopt cylindrical coordinates (r, z) with origin at the centre of the pore and z along the axis of symmetry, together with oblate spherical coordinates (ξ, η) where $\infty > \xi > -\infty$ and $\pi/2 > \eta \geqslant 0$ such that

$$z = a \sinh \xi \cos \eta, \quad r = a \cosh \xi \sin \eta. \tag{2.20a,b}$$

The scale factors are

$$h_\xi = h_\eta = a(\cosh^2 \xi - \sin^2 \eta)^{1/2}. \tag{2.21}$$

The imposed electric field is given by Morse & Feshbach (1953, p. 1292), with potential

$$\chi = \frac{\Delta\phi}{2}\left[1 - \frac{2}{\pi}\tan^{-1}\left(\frac{1}{\sinh \xi}\right)\right]. \tag{2.22}$$

Happel & Brenner (1983, p. 153) give the stream function $\psi = -a^3 \Delta p(1 - \cos^2 \eta)/(6\pi\mu)$ for flow 2. Comparing the resulting velocity, $\bar{\boldsymbol{u}}$, with (2.18), we have

$$G_\xi = -\frac{a \cos^2 \eta}{2\pi\mu \cosh \xi (\cosh^2 \xi - \sin^2 \eta)^{1/2}}, \quad G_\eta = 0. \tag{2.23a,b}$$

Substituting (2.22) and (2.23) into (2.19) yields the electro-osmotic flow rate

$$Q = \frac{2a^3 \Delta\phi}{\pi\mu}\int_0^{\pi/2} \mathrm{d}\eta \int_0^\infty \rho_0 \frac{\cos^2 \eta \sin \eta}{\cosh \xi}\,\mathrm{d}\xi. \tag{2.24}$$

The equilibrium charge density ρ_0 in the linearized, Debye–Hückel limit may be obtained by excising the solution for a uniformly charged disk (Sherwood & Stone 1995) from that for a charged infinite plate. Hence

$$\rho_0 = \sigma\kappa^2 a\left[\int_0^\infty \frac{J_1(as)J_0(rs)}{(\kappa^2 + s^2)^{1/2}}\,\mathrm{e}^{-(\kappa^2+s^2)^{1/2}z}\,\mathrm{d}s - \frac{\mathrm{e}^{-\kappa z}}{\kappa a}\right]. \tag{2.25}$$

The integral in (2.24) cannot be evaluated in closed form when ρ_0 is given by (2.25). However, in the long-Debye-length limit $\kappa a \ll 1$, the rate of decay of $\boldsymbol{G}$ and $\boldsymbol{\nabla}\chi$ is such that the major contribution to the integral in equation (2.24) comes from a region (near the hole) of volume $O(a^3)$, within which $\rho_0 \approx -\sigma\kappa$. Thus,

$$Q \sim -\frac{2a^3 \Delta\phi}{\pi\mu}(\sigma\kappa)\int_0^{\pi/2} \cos^2 \eta \sin \eta\,\mathrm{d}\eta \int_0^\infty \frac{\mathrm{d}\xi}{\cosh \xi} = -\frac{a^3 \kappa\sigma\,\Delta\phi}{3\mu} = \kappa a Q_0, \tag{2.26}$$

where $Q_0 = -a^2\sigma\,\Delta\phi/(3\mu)$ is a convenient characteristic flow rate.

In other cases, the integral must be evaluated numerically. It is convenient to introduce new variables $x = \kappa a$, $t = sa$, $\bar{r} = r/a$, $\bar{z} = z/a$ and $q = \cos \eta$ in terms of which (2.24) becomes

$$Q = \frac{2a^2\sigma\,\Delta\phi}{\mu\pi}\left[-xI_2 + x^2\int_0^{\pi/2} \mathrm{d}\eta \int_0^\infty I_1 \frac{\cos^2 \eta \sin \eta}{\cosh \xi}\,\mathrm{d}\xi\right], \tag{2.27}$$

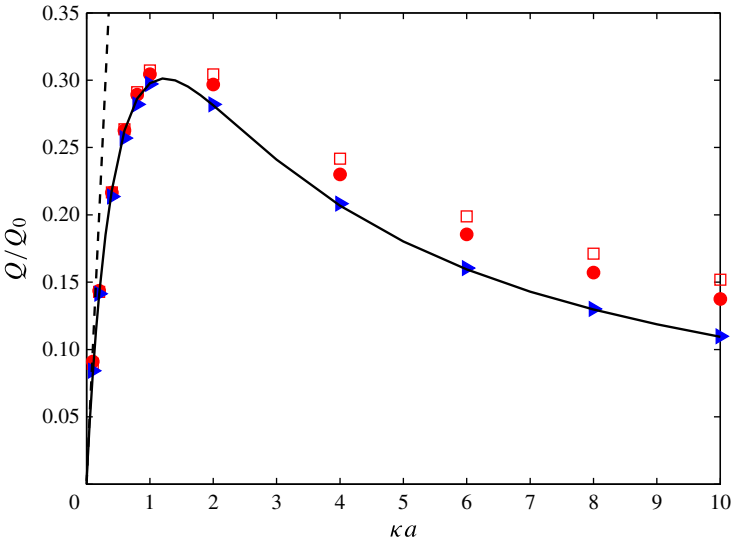

FIGURE 2. (Colour online) The normalized flow rate Q/Q_0 through a circular pore of radius a in a membrane of thickness $h = 0$ as a function of κa determined from (2.27) (solid line), with asymptote $Q/Q_0 \sim \kappa a$ (dashed line) as described by (2.26). The symbols are from the full finite volume simulations of § 3 with $h/a = 0$ (triangles), 0.06 (circles) and 0.1 (squares).

with I_1 and I_2 defined as

$$I_1 = \int_0^\infty \frac{J_1(t)J_0(\bar{r}t)}{\sqrt{x^2+t^2}} \exp\left[-\bar{z}\sqrt{x^2+t^2}\right] \mathrm{d}t, \tag{2.28}$$

$$I_2 = \int_0^1 q^2 \left[ci(xq)\sin(xq) - si(xq)\cos(xq)\right] \mathrm{d}q, \tag{2.29}$$

where $si(\alpha), ci(\alpha)$ are the sine and cosine integrals

$$si(\alpha) = -\int_\alpha^\infty \frac{\sin t}{t}\,\mathrm{d}t, \quad ci(\alpha) = -\int_\alpha^\infty \frac{\cos t}{t}\,\mathrm{d}t. \tag{2.30a,b}$$

The integrals I_1 in (2.28) and I_2 in (2.29) were evaluated using the MATLAB routine `quadgk` (MathWorks 2010). Here I_1 represents the potential due to a thin charged disk, and decays exponentially at large distances, as does $1/\cosh(\xi)$. The ξ integration in (2.27) could therefore be truncated at a large value, taken to be $\xi = 8$ (corresponding to a distance of approximately $1490a$ from the pore). To evaluate the second term in the brackets in (2.27), the (ξ, η) space was divided into subregions, with typically 500 intervals for ξ and 200 for η. Smaller intervals were used near the pore ($\xi \ll 1$) and near the membrane ($\pi/2 - \eta \ll 1$). For every pair (ξ, η), the integral $I_1(\xi, \eta)$ was numerically evaluated and Q was obtained via trapezoidal summation within MATLAB. Results are shown in figure 2, with the asymptotic regime $\kappa a \ll 1$, described by (2.26), depicted by the dashed straight line of unit slope.

3. Flow through a hole in a membrane of finite thickness

In order to examine the validity of (2.27), the full PNP–Stokes system of equations was solved numerically using a finite volume method based on the open-source

computational fluid dynamics (CFD) library OpenFOAM (OpenCFD 2012). Our model has been described by Mao *et al.* (2013), and details of the implementation for the current problem are presented in the Appendix. The cases studied include membranes of thickness $h = 0$ and $h > 0$ in the regime of weak applied fields and low membrane charge. These conditions, stated in § 2.2, may be restated more conveniently as $\hat{\phi}^{-1} \gg \kappa a \gg \hat{\sigma}$ where $\hat{\sigma} = ae|\sigma|/(\epsilon kT)$ and $\hat{\phi} = |\epsilon\Delta\phi/(\sigma a)|$ are dimensionless parameters characterizing the degree of membrane charge and the strength of the applied field, respectively. In the simulations presented here, the values of these parameters were $\hat{\sigma} = 0.273$ and $\hat{\phi} = 0.071$, so that (2.27) can be expected to be a reasonable approximation in the range $14 \gg \kappa a \gg 0.3$.

The computed flow rate Q normalized by $Q_0 = -a^2\sigma\Delta\phi/(3\mu)$ is shown by the symbols in figure 2. Good agreement with (2.27) is obtained, but thicker membranes result in somewhat increased flow rates. The discrepancy increases at shorter Debye lengths.

The analysis of § 2 assumed that effects due to ICEO are negligible. However, Thamida & Chang (2002) have shown that ICEO generates vortices at sharp corners, and such vortices will inevitably be generated in the membrane geometry considered here. In the vicinity of the edge of the nanopore, where $r/a = 1 + s$, the potential χ, given by (2.22), on the membrane surface $z = 0$ may be expanded as

$$\chi = \pm\frac{\Delta\phi}{\pi}\sqrt{2s} \quad \text{on } z = \pm 0. \tag{3.1}$$

If we assume that this potential is little modified when the membrane has a finite thickness $h > 0$, the potential gradient within the solid membrane due to the external potential χ is

$$\frac{\partial\phi_s}{\partial z} = \frac{2\Delta\phi}{\pi}\frac{\sqrt{2s}}{h}, \tag{3.2}$$

and if $\epsilon_s \ll \epsilon$ the induced potential gradient normal to the surface within the liquid is $(\epsilon_s/\epsilon)\partial\phi_s/\partial z$. This corresponds to an induced surface charge (with accompanying charge cloud of counter-ions)

$$\sigma_i = \mp\frac{2\epsilon_s\Delta\phi}{\pi}\frac{\sqrt{2s}}{h} \quad \text{on } z = \pm 0. \tag{3.3}$$

The analysis breaks down when $s \lesssim h/a$, in which case the detailed geometry near the edge of the pore becomes important. If the membrane has rounded edges, the curvature is approximately h^{-1} and the induced charge is at most $\sigma_i \sim \epsilon_s\Delta\phi/(ah)^{1/2}$; this may be neglected as long as it is small compared to σ or, equivalently, if $(\epsilon_s/\epsilon)\sqrt{(a/h)}\,\hat{\phi} \ll 1$. For common membrane materials (e.g. lipids and silica), $\epsilon_s/\epsilon \sim 0.1$; thus, as long as the applied field remains weak, ICEO effects are restricted to the neighbourhood of sharp corners.

The results of full numerical solutions of the PNP–Stokes equations reported in figure 2 were computed with membrane permittivity $\epsilon_s = 0$. However, it is shown in the Appendix that numerical solutions for appropriate non-zero solid permittivities $\epsilon_s > 0$ predict flow rates Q that differ little from those with $\epsilon_s = 0$ in the parameter regime under consideration. The contribution of such effects to the net fluid flux, Q, is at best very weak. This is perhaps not surprising, since even when (as here) there are sharp corners, if the membrane is uncharged and the electrolyte is symmetric (with identical ionic mobilities), symmetry dictates that ICEO cannot generate a net flow Q through the pore. So although nonlinear effects such as ICEO can generate a net fluid

flow through a charged membrane, the applied field $\Delta\phi$ must be larger than the fields considered here. An ICEO contribution to the fluid flux is in principle possible, but only for a charged membrane at high applied fields, as, for example, in the numerical results presented by Mao *et al.* (2013).

The reciprocal theorem used in § 2.2 enabled us to determine the volumetric flow rate Q through the pore without a full computation of the velocity field. This has the advantage of leading quickly to a value for Q. However, this approach hides other interesting features of the flow, such as eddies, whether generated by ICEO (Thamida & Chang 2002) or by the pore throat restricting the flow (Park *et al.* 2006). These features are only revealed by full numerical computations, such as those discussed in the Appendix.

3.1. *The limits of thick and thin membranes*

Since the fluid flux through the pore is generated by the applied potential $\Delta\phi$, we can define an 'electro-osmotic conductance' $H = Q/\Delta\phi$ in analogy to the electric conductance. If the membrane thickness is such that $h \gg a$, we have a long cylindrical pore with surface charge density σ at the wall. The electro-osmotic flow velocity is then (Levine *et al.* 1975)

$$u = \frac{\epsilon E_0}{\mu}[\phi_0 - \zeta], \tag{3.4}$$

where $\phi_0 = -\epsilon\kappa^2\rho_0$ is the equilibrium potential in the double layer, ζ is the equilibrium potential at the wall and $E_0 = \Delta\phi/h$. The equilibrium potential of a cylindrical pore in the Debye–Hückel limit is

$$\phi_0 = \zeta\frac{I_0(\kappa r)}{I_0(\kappa a)} = \frac{\sigma}{\epsilon\kappa}\frac{I_0(\kappa r)}{I_1(\kappa a)}. \tag{3.5}$$

Integrating the fluid velocity u in (3.4) over the cross-section, we obtain the volumetric flow rate Q and hence the electro-osmotic conductance (Rice & Whitehead 1965)

$$H_c = \frac{Q}{\Delta\phi} = \frac{2\pi\sigma a^3}{\mu h}\left[\frac{1}{(\kappa a)^2} - \frac{1}{2(\kappa a)}\frac{I_0(\kappa a)}{I_1(\kappa a)}\right]. \tag{3.6}$$

On the other hand, when the thickness is such that $h/a \ll 1$, we expect the system to be identical to a hole in a zero-thickness membrane, and the electro-osmotic conductance may be obtained, using (2.27), as

$$H_p = \frac{Q}{\Delta\phi} = \frac{2\sigma a^2}{\mu\pi}\left[-(\kappa a)I_2 + (\kappa a)^2\int_0^{\pi/2}\mathrm{d}\eta\int_0^{\infty} I_1\frac{\cos^2\eta\sin\eta}{\cosh\xi}\,\mathrm{d}\xi\right]. \tag{3.7}$$

3.2. *The electro-osmotic access resistance of a nanopore*

If a membrane of thickness h containing a circular hole of radius a separates two uniformly conducting regions, then the electrical resistance of the cylindrical hole increases proportional to h. This might suggest a vanishing resistance for an infinitely thin membrane. However, in reality, as $h \to 0$ the electrical resistance is dominated by entrance and exit effects, and can be determined from the electrical potential (2.22). This is called the 'access resistance' of the pore, and for a circular pore in an infinitely thin membrane it is described by a simple analytical formula (Hall 1975).

An analogous situation applies to the problem of electro-osmotic flow through a pore in a membrane. When the pore length h is large compared to the pore radius a,

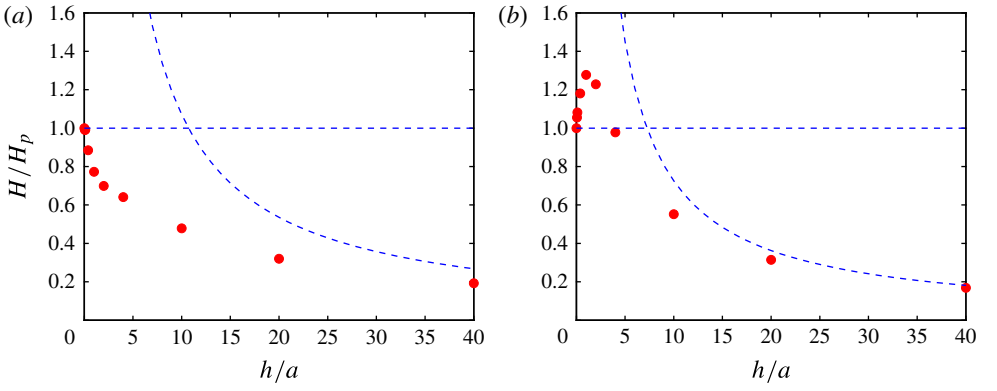

FIGURE 3. (Colour online) The normalized 'electro-osmotic conductance' H/H_p determined from the full numerical simulation (circles) as a function of the normalized membrane thickness h/a, in the cases where (*a*) $\kappa a = 0.4$ and (*b*) $\kappa a = 2.0$. The dashed lines correspond to the thin ($H = H_p$) and thick ($H = H_c$) membrane limits obtained from (3.6) and (3.7).

the flow conductance is such that $H \sim H_c \sim h^{-1}$ from (3.6), a consequence of the fact that the electric field in the pore satisfies $E \sim \Delta\phi/h$. However, H does not increase indefinitely as $h \to 0$ but instead approaches a finite value H_p given by (3.7). The surface charge $2\pi ah\sigma$ within the cylindrical pore goes to zero as $h \to 0$. Electro-osmotic motion is therefore determined by flow in the fluid on either side of the membrane, as described in § 2, and not by the cylindrical pore. Thus, in analogy to the corresponding electrical problem, H_p^{-1} may be regarded as an 'access resistance' of the pore to electro-osmotic flow.

Figure 3 shows the electro-osmotic conductance H obtained from the finite volume numerical computations as a function of h/a. The computed value of H is normalized by H_p obtained from (3.7). It is seen that H/H_p approaches unity as $h/a \to 0$ and approaches $H_c/H_p \sim h^{-1}$ for large h/a. The dashed line representing H_c/H_p was obtained from (3.6) and (3.7). The results of the full computations indicate that although H does exhibit the expected limiting behaviours, it does not vary monotonically with h at short Debye lengths. The origin of the peak at intermediate values of h/a will be investigated further in future work.

4. Concluding remarks

We have assumed that the surface charge density σ is sufficiently low that the zeta potential is small, $\zeta \ll kT/e \approx 25$ mV at $T = 298$ K. Thus, the Poisson–Boltzmann equation can be linearized. Non-dimensional zeta potentials $e\zeta/kT$ in colloidal systems, though not always small, are typically at most 5, and it is found that theories based on small potentials usually give useful qualitative insight into electrokinetic behaviour over this range of potentials (e.g. Levine *et al.* 1975).

We have also assumed that the applied potential difference satisfies $\Delta\phi \ll \zeta$. Potential differences applied in experiments are typically of the same order as typical zeta potentials, which in silica substrates vary in magnitude between 0 and 100 mV, depending mainly on counter-ion concentration (Kirby & Hasselbrink 2004*a*,*b*). For example, Keyser *et al.* (2006) described experiments in which $\Delta\phi$ was in the range 30–100 mV. Nanopores (with radius approximately 5–10 nm) in graphene sheets have recently been used in DNA translocation experiments

(Garaj *et al.* 2010; Merchant *et al.* 2010; Schneider *et al.* 2010). The applied voltage $\Delta\phi$ was in the range 0–200 mV in these experiments. The computations of Mao *et al.* (2013) predict that the electro-osmotic flow rate through a pore in a membrane varies nonlinearly with $\Delta\phi$ only at voltages greater than 100 mV. Thus, we again expect the results presented here to give at least a qualitative understanding of electro-osmotic flow in such experiments.

Electro-osmotic flow through nanopores has been shown to control the translocation velocity of charged polymers in resistive pulse experiments (Ghosal 2006, 2007*a*). When the free translocation of the polymer is hindered by tethering it to a colloid held in an optical trap, the tethering force has been shown to be determined by the electro-osmotic flow within the pore (Keyser *et al.* 2006; Ghosal 2007*b*; Laohakunakorn *et al.* 2013*a*). Furthermore, it has been argued that the flow outside and in the vicinity of the nanopore controls the capture rate of polymers into the pore (Wong & Muthukumar 2007), though the experimental evidence for this appears tentative at present.

In addition to the single-molecule experiments mentioned above, our results should also be helpful in understanding the properties of nanoporous membranes that are used in batteries, water desalination and numerous other industrial applications. Gadaleta *et al.* (2014) have recently studied the electrical conductivity of a model membrane consisting of an array of nanopores. However, the applied voltage should also result in an electro-osmotic flux, the calculation of which may be undertaken as a suitable generalization of the approach presented here. Since membrane-bound organelles in cells contain nanopores that control the traffic of biological molecules across the membrane, our results may also be of interest in the biological context (see e.g. Gu, Cheley & Bayley 2003).

Acknowledgements

M.M. & S.G. acknowledge support from the NIH through grant 4R01HG004842-03. SG was hosted by the Cavendish Laboratory, University of Cambridge, as a visiting professor with funds provided by the Leverhulme Trust. JDS thanks the Department of Applied Mathematics and Theoretical Physics of the University of Cambridge and the Institut de Mécanique des Fluides de Toulouse for hospitality.

Appendix. Numerical solution of the PNP–Stokes equations

A.1. *Numerical scheme*

An electrohydrodynamic solver was developed to solve the PNP–Stokes system of equations using the finite volume method. The solver was based on the OpenFOAM CFD library (OpenCFD 2012), a C++ library designed for computational mechanics, containing a collection of object-oriented classes developed to represent mesh, fields, matrices and the necessary operations on fields and tensors. It also provides functions to handle finite volume discretization and matrix equation solving.

The time-independent PNP–Stokes equations are

$$\epsilon\nabla^2\phi + \sum_{i=1}^{N} z_i e n^i = 0, \tag{A 1}$$

$$\boldsymbol{\nabla}\cdot\left[n^i\boldsymbol{u} - \omega^i(kT\boldsymbol{\nabla}n^i + ez_i n^i\boldsymbol{\nabla}\phi)\right] = 0, \tag{A 2}$$

$$-\boldsymbol{\nabla}p + \mu\nabla^2\boldsymbol{u} - \boldsymbol{\nabla}\phi\sum_{i=1}^{N} z_i e n^i = \boldsymbol{0}, \tag{A 3}$$

$$\boldsymbol{\nabla}\cdot\boldsymbol{u} = 0. \tag{A 4}$$

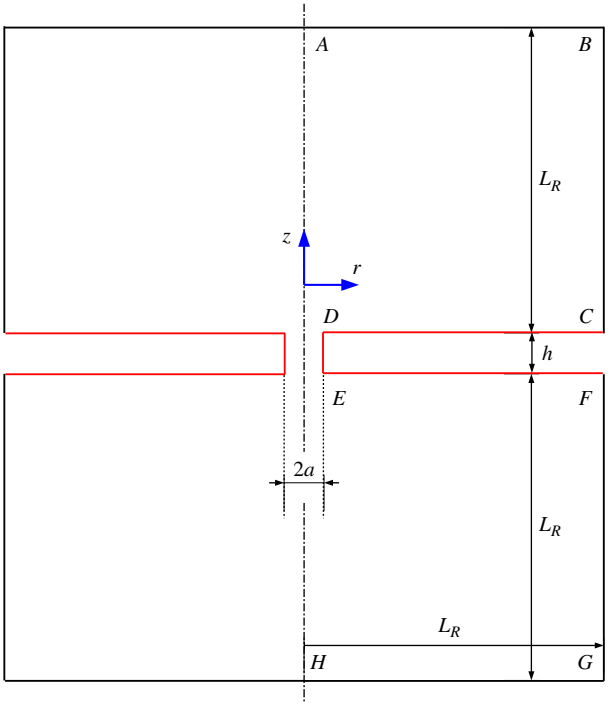

FIGURE 4. (Colour online) A sketch of the axisymmetric geometry used in the simulation.

In our simulation we consider a 1–1 symmetric electrolyte solution containing ions with equal mobilities. The boundary conditions to be satisfied by the solution are discussed in appendix A.2.

We apply the following scheme to solve the PNP–Stokes equations. We start from a zero flow field. Equations (A 1) and (A 2) are solved sequentially in a loop with under-relaxation until the absolute residual is smaller than 10^{-6}. Under-relaxation is necessary because the PNP system is nonlinear. The electric volume force $-\nabla\phi \sum_i z_i e n^i$ is obtained from this solution and used explicitly in the next step, i.e. the solution of the incompressible Stokes flow, (A 3) and (A 4). The SIMPLE algorithm is used with a fixed volume force density. The flow field is then substituted into (A 2). The PNP equations are then solved again using the updated flow field. An outer loop is constructed to iterate over the PNP loop and the Stokes flow module.

For the finite volume discretization of the governing equations, central differences are used for all diffusive terms in (A 2) and viscous terms in (A 3). A second-order upwind scheme is used for the convective terms in (A 2). The discretized linear system is solved using a preconditioned conjugate gradient solver if the matrix is symmetric or a preconditioned biconjugate gradient solver if the matrix is asymmetric. The details of the numerical algorithm are given by Ferziger & Perić (2002).

A.2. *Mathematical model of the nanopore*

A schematic view of the axisymmetric geometry used for the full numerical simulations is provided in figure 4. It consists of a circular hole of radius a in a solid dielectric membrane $CDEF$ of arbitrary thickness $h \geqslant 0$. The membrane surfaces CD, DE and EF have a uniform surface charge density σ. Two large cylindrical

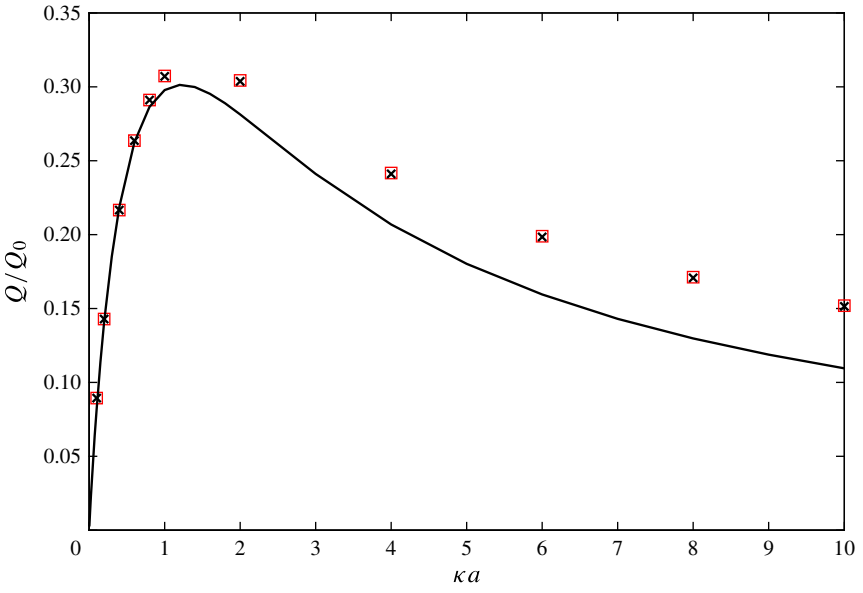

FIGURE 5. (Colour online) The normalized flow rate through a circular pore of radius a in a thin membrane as a function of κa. The solid line shows results for a membrane of zero thickness, obtained via the reciprocal theorem and (2.24). The symbols are from the full numerical simulation with a membrane of thickness $h = 0.1a$: squares show results for a non-polarizable membrane with $\epsilon_s = 0$, and crosses show results for a membrane with a dielectric constant of 3.9; the dielectric constant of the electrolyte is 80. The effect on the flow rate due to membrane polarizability and consequent ICEO is seen to be negligible.

reservoirs are connected to the pore, one at each end. The length and radius of both the reservoirs are identical, and are $L_R = \max(10a, 10\kappa^{-1})$, chosen to be much larger than either the hole radius a or the Debye length κ^{-1} in order to approximate an infinite reservoir.

We adopt the following boundary conditions (Mao *et al.* 2013). The ion number densities on AB and GH are constant and equal to the number density n_∞ in the bulk solution far from any charged surfaces. The electrical potentials are uniform on AB and on GH, with a potential difference of $\Delta\phi$ between the top (AB) and the bottom (GH). The pressure p_∞ on AB is uniform and equal to that on GH. On the side walls BC and FG, the radial electric field, radial ionic fluxes and radial velocity, which decay away from the pore, are set to zero. A zero tangential shear stress is imposed on flow parallel to the side walls. At the membrane surfaces CD, DE and EF, a no-flux condition is used for (A 2), and a no-slip condition for the flow; the electric field $\boldsymbol{E}$ undergoes a jump across the solid–fluid interface such that $\epsilon \boldsymbol{E}\cdot\hat{\boldsymbol{n}} - \epsilon_s \boldsymbol{E}_s\cdot\hat{\boldsymbol{n}} = \sigma$, where ϵ is the electrical permittivity of the fluid, ϵ_s is the permittivity of the membrane, $\boldsymbol{E}_s$ is the electric field at the interface within the membrane and $\hat{\boldsymbol{n}}$ is the unit normal at the surface directed into the fluid. The potential is continuous across the interface.

The strength of the applied field and the amount of surface charge can be characterized by the dimensionless parameters $\hat{\phi} = |\epsilon\Delta\phi/(\sigma a)|$ and $\hat{\sigma} = ae|\sigma|/(\epsilon kT)$, respectively. In the simulations presented here, the values of these parameters were kept fixed at $\hat{\phi} = 0.071$ and $\hat{\sigma} = 0.273$. The flow rate Q was obtained by numerically integrating the z-component of the velocity over the plane $z = 0$.

A.3. *Effect of membrane polarizability*

If the membrane polarizability is sufficiently small so that $|\epsilon_s \boldsymbol{E}_s \cdot \hat{\boldsymbol{n}}| \ll |\epsilon \boldsymbol{E} \cdot \hat{\boldsymbol{n}}|$, then the jump condition of the normal component of the field may be replaced by $\epsilon \boldsymbol{E} \cdot \hat{\boldsymbol{n}} = \sigma$. In this case, the computational domain may be restricted to include only the fluid phase. This approximation was adopted for the results presented in figures 2 and 3. Thus, effects due to ICEO were neglected. The results of a calculation to test the validity of this assumption in the parameter range of interest are shown in figure 5. The data from figure 2 for a non-polarizable membrane of thickness $h = 0.1a$ are reproduced in figure 5. For comparison, the result of a second calculation in which the dielectric constant of the membrane material was set to 3.9 (corresponding to silica) is also shown. The electrolyte is considered polarizable with a dielectric constant of 80. It is seen that the effect of membrane polarizability on the flow rate is negligible.

REFERENCES

ALBERTS, B., BRAY, D., LEWIS, J., RAFF, M., ROBERTS, K. & WATSON, J. D. 1994 *Molecular Biology of the Cell*. Garland Science, Taylor & Francis.

CHANG, H. C. & YOSSIFON, G. 2009 Understanding electrokinetics at the nanoscale: a perspective. *Biomicrofluidics* **3** (1), 012001.

CHANG, H. C., YOSSIFON, G. & DEMEKHIN, E. A. 2012 Nanoscale electrokinetics and microvortices: how microhydrodynamics affects nanofluidic ion flux. *Annu. Rev. Fluid Mech.* **44**, 401–426.

VAN DORP, S., KEYSER, U. F., DEKKER, N. H., DEKKER, C. & LEMAY, S. 2009 Origin of the electrophoretic force on DNA in solid-state nanopores. *Nat. Phys.* **5** (5), 347–351.

FERZIGER, J. H. & PERIĆ, M. 2002 *Computational Methods for Fluid Dynamics*. Springer.

GADALETA, A., SEMPERE, C., GRAVELLE, S., SIRIA, A., FULCRAND, R., YBERT, C. & BOCQUET, L. 2014 Sub-additive ionic transport across arrays of solid-state nanopores. *Phys. Fluids* **26** (1), 012005.

GARAJ, S., HUBBARD, W., REINA, A., KONG, J., BRANTON, D. & GOLOVCHENKO, J. 2010 Graphene as a subnanometre trans-electrode membrane. *Nature* **467** (7312), 190–193.

GHOSAL, S. 2006 Electrophoresis of a polyelectrolyte through a nanopore. *Phys. Rev.* E **74** (4), 041901.

GHOSAL, S. 2007*a* Effect of salt concentration on the electrophoretic speed of a polyelectrolyte through a nanopore. *Phys. Rev. Lett.* **98** (23), 238104.

GHOSAL, S. 2007*b* Electrokinetic-flow-induced viscous drag on a tethered DNA inside a nanopore. *Phys. Rev.* E **76** (6), 061916.

GU, L., CHELEY, S. & BAYLEY, H. 2003 Electro-osmotic enhancement of the binding of a neutral molecule to a transmembrane pore. *Proc. Natl Acad. Sci. USA* **100** (26), 15498–15503.

HALL, J. E. 1975 Access resistance of a small circular pore. *J. Gen. Physiol.* **66**, 531–532.

HALL, A. R., SCOTT, A., ROTEM, D., MEHTA, K., BAYLEY, H. & DEKKER, C. 2010 Hybrid pore formation by directed insertion of α-haemolysin into solid-state nanopores. *Nat. Nanotechnol.* **5** (12), 874–877.

HAPPEL, J. & BRENNER, H. 1983 *Low Reynolds Number Hydrodynamics: with Special Applications to Particulate Media*. Martinus Nijhoff Publishing.

HENRY, D. C. 1931 The cataphoresis of suspended particles. Part 1. The equation of cataphoresis. *Proc. R. Soc. Lond.* A **133** (821), 106–129.

HU, G., MAO, M. & GHOSAL, S. 2012 Ion transport through a graphene nanopore. *Nanotechnology* **23** (39), 395501.

KASIANOWICZ, J. J., BRANDIN, E., BRANTON, D. & DEAMER, D. W. 1996 Characterization of individual polynucleotide molecules using a membrane channel. *Proc. Natl Acad. Sci. USA* **93** (24), 13770–13773.

KEYSER, U. F., KOELEMAN, B. N., VAN DORP, S., KRAPF, D., SMEETS, R., LEMAY, S., DEKKER, N. & DEKKER, C. 2006 Direct force measurements on DNA in a solid-state nanopore. *Nat. Phys.* **2** (7), 473–477.

KIRBY, B. J. & HASSELBRINK, E. F. 2004*a* Zeta potential of microfluidic substrates: 1. Theory, experimental techniques, and effects on separations. *Electrophoresis* **25**, 187–202.

KIRBY, B. J. & HASSELBRINK, E. F. 2004*b* Zeta potential of microfluidic substrates: 2. Data for polymers. *Electrophoresis* **25**, 203–213.

KÜNKELE, K. P., HEINS, S. & DEMBOWSKI, M. 1998 The preprotein translocation channel of the outer membrane of mitochondria. *Cell* **93**, 1009–1019.

LAOHAKUNAKORN, N., GHOSAL, S., OTTO, O., MISIUNAS, K. & KEYSER, U. F. 2013*a* DNA interactions in crowded nanopores. *Nano Lett.* **13** (6), 2798–2802.

LAOHAKUNAKORN, N., GOLLNICK, B., MORENO-HERRERO, F., AARTS, D., DULLENS, R., GHOSAL, S. & KEYSER, U. F. 2013*b* A Landau–Squire nanojet. *Nano Lett.* **13** (11), 5141–5146.

LEVINE, S., MARRIOTT, J. R., NEALE, G. & EPSTEIN, N. 1975 Theory of electrokinetic flow in fine cylindrical capillaries at high zeta-potentials. *J. Colloid Interface Sci.* **52** (1), 136–149.

LI, J., GERSHOW, M., STEIN, D., BRANDIN, E. & GOLOVCHENKO, J. 2003 DNA molecules and configurations in a solid-state nanopore microscope. *Nat. Mater.* **2** (9), 611–615.

MAO, M., GHOSAL, S. & HU, G. 2013 Hydrodynamic flow in the vicinity of a nanopore induced by an applied voltage. *Nanotechnology* **24** (24), 245202.

MARTIN, J., MAHLKE, K. & PFANNER, N. 1991 Role of an energized inner membrane in mitochondrial protein import: $\delta\psi$ drives the movement of presequences. *J. Biol. Chem.* **266**, 18051–18057.

MATHWORKS 2010 MATLAB version 7.10.0 (R2010a). The MathWorks Inc.

MATOUSCHEK, A., PFANNER, N. & VOOS, W. 2000 Protein unfolding by mitochondria: the Hsp70 import motor. *EMBO Rep.* **1**, 404–410.

MERCHANT, C., HEALY, K., WANUNU, M., RAY, V., PETERMAN, N., BARTEL, J., FISCHBEIN, M., VENTA, K., LUO, Z., JOHNSON, A. & DRNDIĆ, M. 2010 DNA translocation through graphene nanopores. *Nano Lett.* **10** (8), 2915–2921.

MORSE, P. & FESHBACH, H. 1953 *Methods of Theoretical Physics*. McGraw-Hill.

MURTSOVKIN, V. A. 1996 Nonlinear flows near polarized disperse particles. *Colloid J.* **58**, 341–349.

OPENCFD 2012 *OpenFOAM – The Open Source CFD Toolbox: User Guide*. 2nd edn. OpenCFD Ltd.

PARK, S. Y., RUSSO, C. J., BRANTON, D. & STONE, H. A. 2006 Eddies in a bottleneck: an arbitrary Debye length theory for capillary electro-osmosis. *J. Colloid Interface Sci.* **297** (2), 832–839.

PFANNER, N. & NEUPERT, W. 1990 The mitochondrial protein import apparatus. *Annu. Rev. Biochem.* **59**, 331–353.

RICE, C. L. & WHITEHEAD, R. 1965 Electrokinetic flow in a narrow cylindrical capillary. *J. Phys. Chem.* **69**, 4017–4024.

RUBINSTEIN, I. & SHTILMAN, L. 1979 Voltage against current curves of cation exchange membranes. *J. Chem. Soc. Faraday Trans.* 2*: Mol. Chem. Phys.* **75**, 231–246.

SAVILLE, D. A. 1977 Electrokinetic effects with small particles. *Annu. Rev. Fluid Mech.* **9**, 321–337.

SCHNEIDER, G. F., KOWALCZYK, S., CALADO, V., PANDRAUD, G., ZANDBERGEN, H., VANDERSYPEN, L. & DEKKER, C. 2010 DNA translocation through graphene nanopores. *Nano Lett.* **10** (8), 3163–3167.

SHERWOOD, J. D. & STONE, H. A. 1995 Electrophoresis of a thin charged disk. *Phys. Fluids* **7** (4), 697–705.

SIWY, Z. S. 2006 Ion-current rectification in nanopores and nanotubes with broken symmetry. *Adv. Funct. Mater.* **16** (6), 735–746.

SIWY, Z. S. & FULINSSKI, A. 2004 A nanodevice for rectification and pumping ions. *Am. J. Phys.* **72** (5), 567–574.

SMEETS, R. M. M., KEYSER, U. F., KRAPF, D., WU, M. Y., DEKKER, N. H. & DEKKER, C. 2006 Salt dependence of ion transport and DNA translocation through solid-state nanopores. *Nano Lett.* **6** (1), 89–95.

SQUIRES, T. M. & BAZANT, M. Z. 2004 Induced-charge electro-osmosis. *J. Fluid Mech.* **509**, 217–252.

STORM, A. J., CHEN, J. H., ZANDBERGEN, H. W. & DEKKER, C. 2005*a* Translocation of double-strand DNA through a silicon oxide nanopore. *Phys. Rev.* E **71** (5), 051903.

STORM, A. J., STORM, C., CHEN, J. H., ZANDBERGEN, H., JOANNY, J. F. & DEKKER, C. 2005*b* Fast DNA translocation through a solid-state nanopore. *Nano Lett.* **5** (7), 1193–1197.

THAMIDA, S. K. & CHANG, H. C. 2002 Nonlinear electrokinetic ejection and entrainment due to polarization at nearly insulated wedges. *Phys. Fluids* **14** (12), 4315–4328.

VLASSIOUK, I. & SIWY, Z. S. 2007 Nanofluidic diode. *Nano Lett.* **7** (3), 552–556.

VLASSIOUK, I., SMIRNOV, S. & SIWY, Z. 2008*a* Nanofluidic ionic diodes: comparison of analytical and numerical solutions. *ACS Nano* **2** (8), 1589–1602.

VLASSIOUK, I., SMIRNOV, S. & SIWY, Z. S. 2008*b* Ionic selectivity of single nanochannels. *Nano Lett.* **8** (7), 1978–1985.

WONG, C. T. A. & MUTHUKUMAR, M. 2007 Polymer capture by electro-osmotic flow of oppositely charged nanopores. *J. Chem. Phys.* **126** (16), 164903.

YOSSIFON, G. & CHANG, H. C. 2008 Selection of nonequilibrium overlimiting currents: universal depletion layer formation dynamics and vortex instability. *Phys. Rev. Lett.* **101** (25), 254501.

ZALTZMAN, B. & RUBINSTEIN, I. 2007 Electro-osmotic slip and electroconvective instability. *J. Fluid Mech.* **579**, 173–226.